# Dynamical $Ag^{+}$-Intercalation with $AgSnSe_2$ Nano-Precipitates in Cl-Doped Polycrystalline $SnSe_2$ toward Ultra-High Thermoelectric Performance

Chengyan Liu,[a] Zhiwei Huang,[b] Dianhui Wang,[a] Xiuxia Wang,[a] Lei Miao,[a,*] Xiaoyang Wang,[a] Shaohai Wu,[a] Nozomu Toyama,[c,d] Toru Asaka,[c,d] Junliang Chen,[a] Eiji Nishibori,[e] Li-Dong Zhao[b,*]

[a]Guangxi Key Laboratory of Information Materials, Guangxi Collaborative Innovation Center of Structure and Property for New Energy and Material, School of Material Science and Engineering, Guilin University of Electronic Technology, Guilin, 541004, China. E-mail: miaolei@guet.edu.cn

[b]School of Materials Science and Engineering, Beihang University, Beijing, 100191, China. E-mail: zhaolidong@buaa.edu.cn

[c]Department of Advanced Ceramics, Nagoya Institute of Technology, Gokiso, Showa, Nagoya, Aichi, 466-8555, Japan

[d]Frontier Research Institute for Materials Science (FRIMS), Nagoya Institute of Technology, Gokiso, Showa, Nagoya, Aichi, 466-8555, Japan.

[e]Division of Physics, Faculty of Pure and Applied Science &, Tsukuba Research Center for Energy Materials Science (TREMS), University of Tsukuba, 1-1-1 Tennodai, Tsukuba, Ibaraki 305-8576, Japan

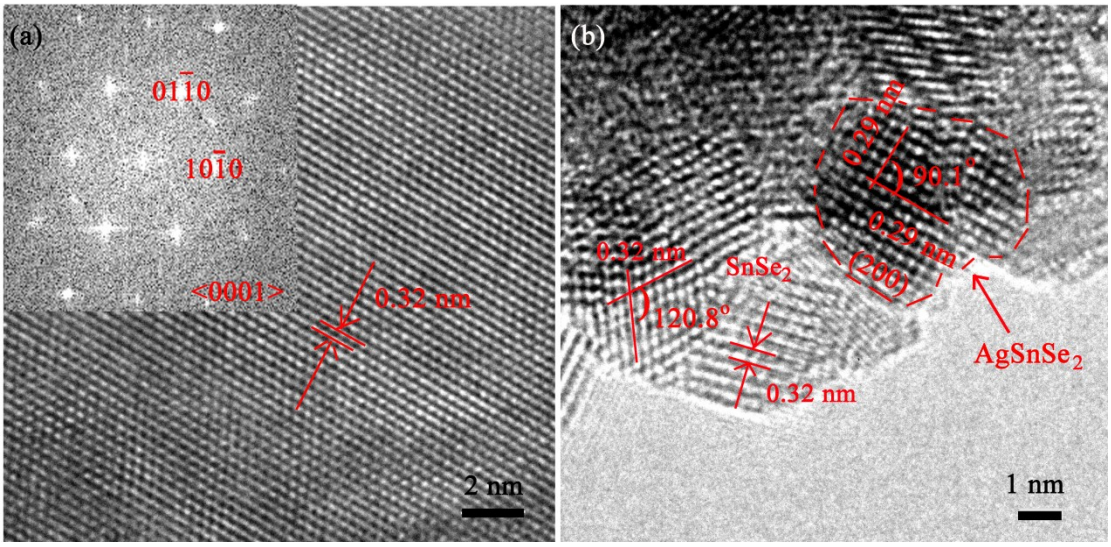


Fig. S1 Typical HRTEM images of the hydrothermal products with atomic (a) 0% and (b) 3% Ag-introduction. The inset in a is the corresponding FFT pattern.

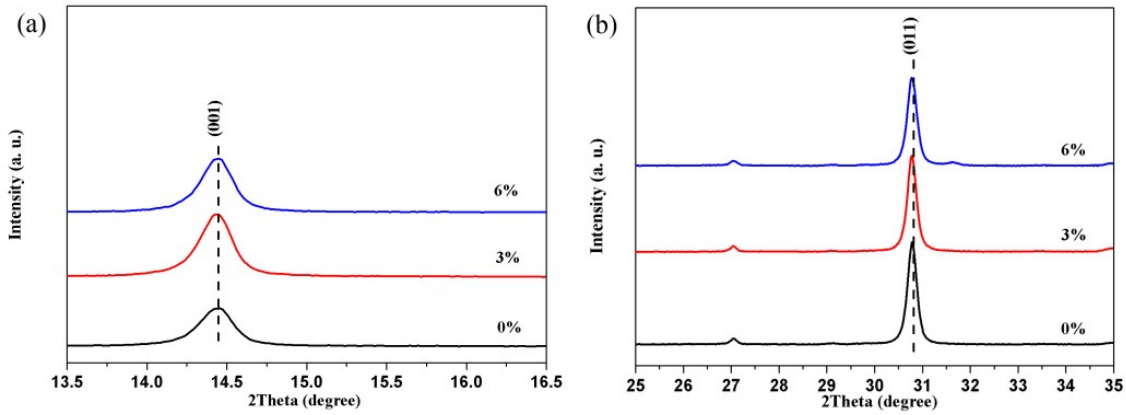


Fig. S2 Expanded view of XRD patterns in Fig. 1(b): (a) 13.5-16.5° and (b) 25-35°.

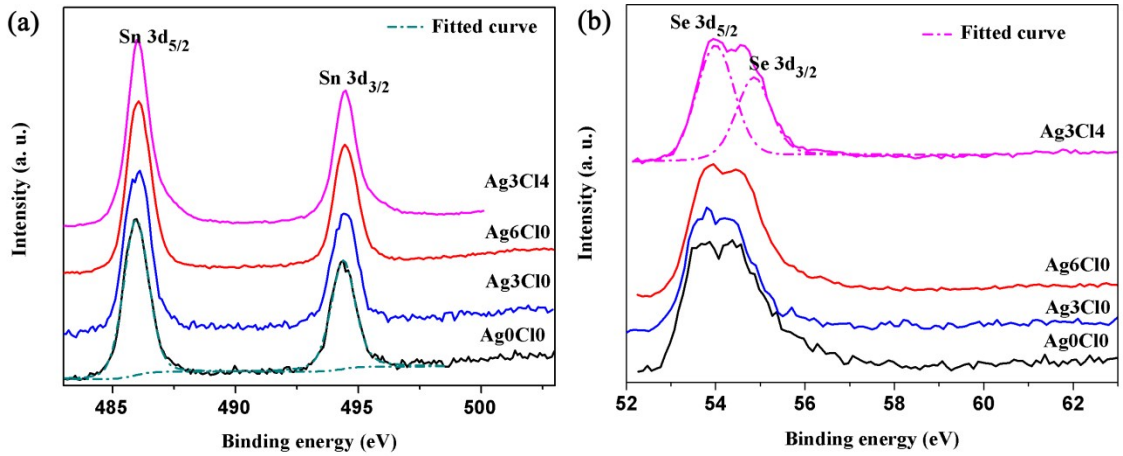


Fig. S3 High-resolution XPS of (a) Sn 3d and (b) Se 3d for the hot-pressed samples.

The binding energies of Sn $3d_{5/2}$ and Sn $3d_{3/2}$ are located at 494.4 eV and 485.9 eV (Fig. S3(a)),

respectively, suggesting that the chemical valence state of Sn is +4.[1] The high-resolution XPS spectrum of Se shows that the binding energies of Se $d_{5/2}$ and Se $3d_{3/2}$ are located at 54.1 eV and 55.2 eV, respectively, which may correspond to $Se^{2-}$ bonded to $Sn^{4+}$.[2]

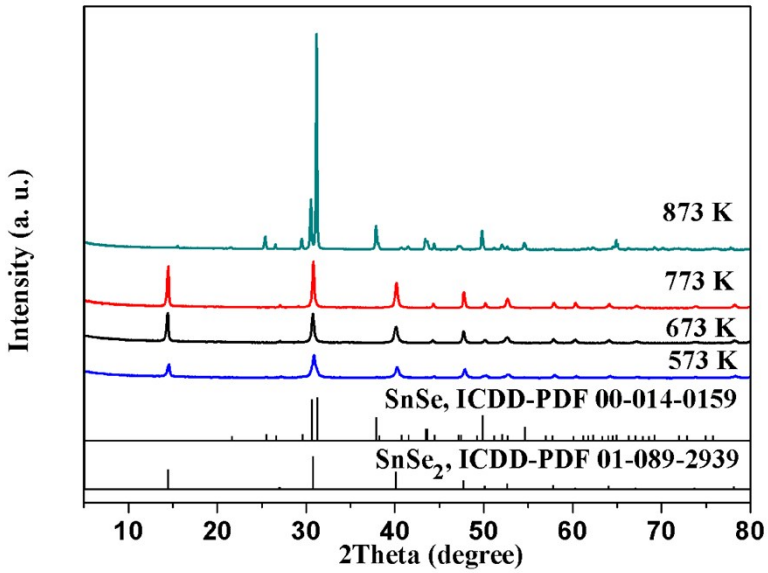


Fig. S4 XRD patterns of the sample Ag0Cl0 (grinded powders) after heat-treating process at different temperature.

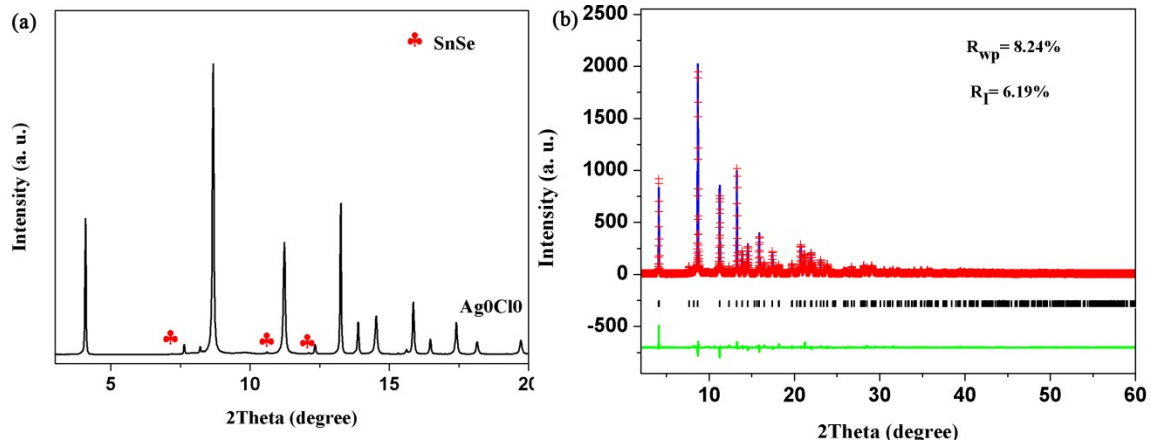


Fig. S5 (a) SR-XRD pattern of the sample Ag0Cl0 (grinded powders) after heat-treating process at 673 K. (b) The corresponding Rietveld refinement result with $R_{wp}$=8.24% and $R_I$=6.19%.

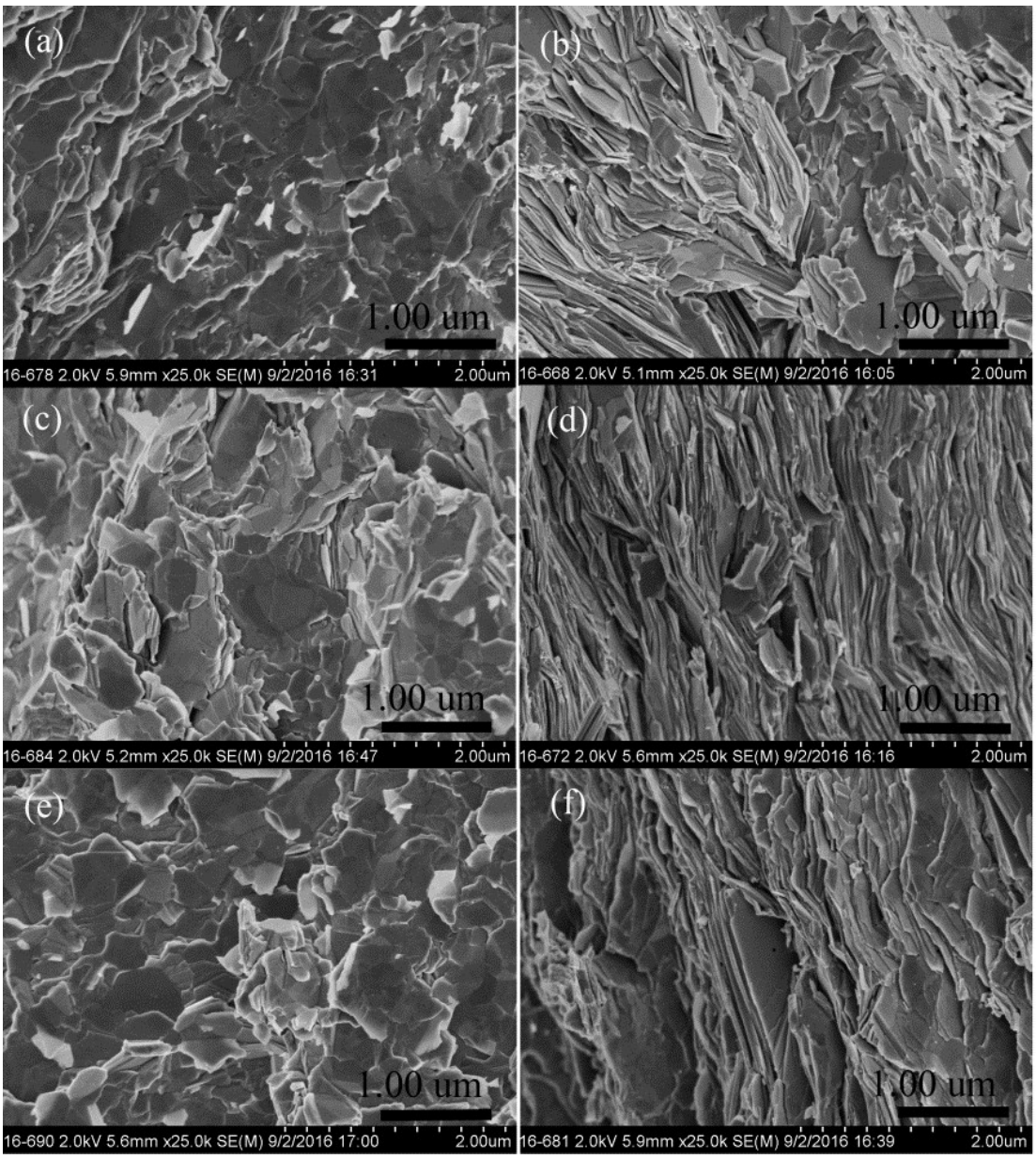


Fig. S6 Typical SEM images of the sample (a-b) Ag0Cl0, (c-d) Ag3Cl0 and (e-f) Ag3Cl4.The left side images were observed on the fracture surfaces perpendicular to the pressing direction while the right side ones were performed on the fracture surfaces parallel to the pressing direction.

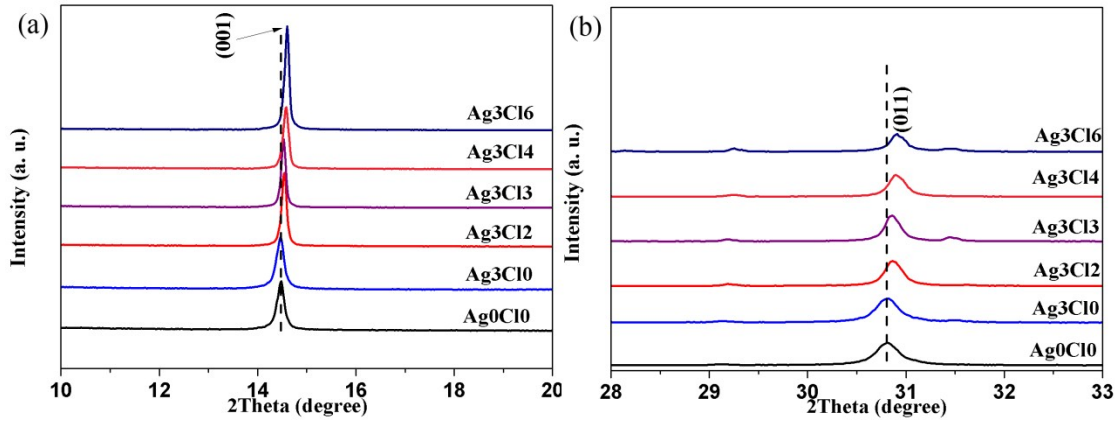


Fig. S7 Expanded view of XRD patterns in Fig. 2(b): (a) 10-20° and (b) 28-33°.

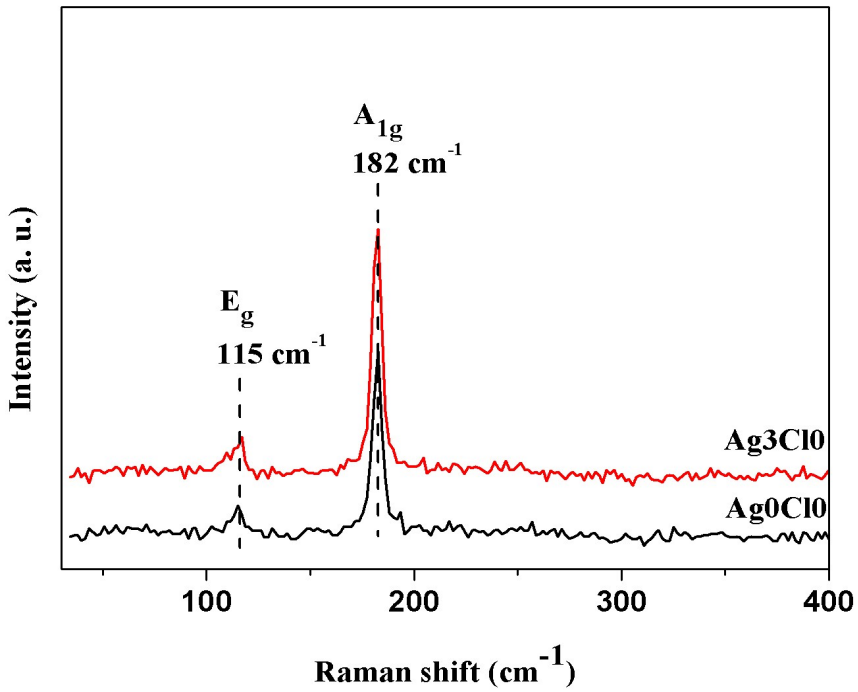


Fig. S8 Raman spectra of the sample Ag0Cl0 and Ag3Cl0.

The peaks at 115 $cm^{-1}$ and 182 $cm^{-1}$ (Fig. S9) can be attributed to the $E_g$ mode (in plane vibration) and $A_{1g}$ mode (out of plane vibration) of $SnSe_2$, respectively.[1,3]

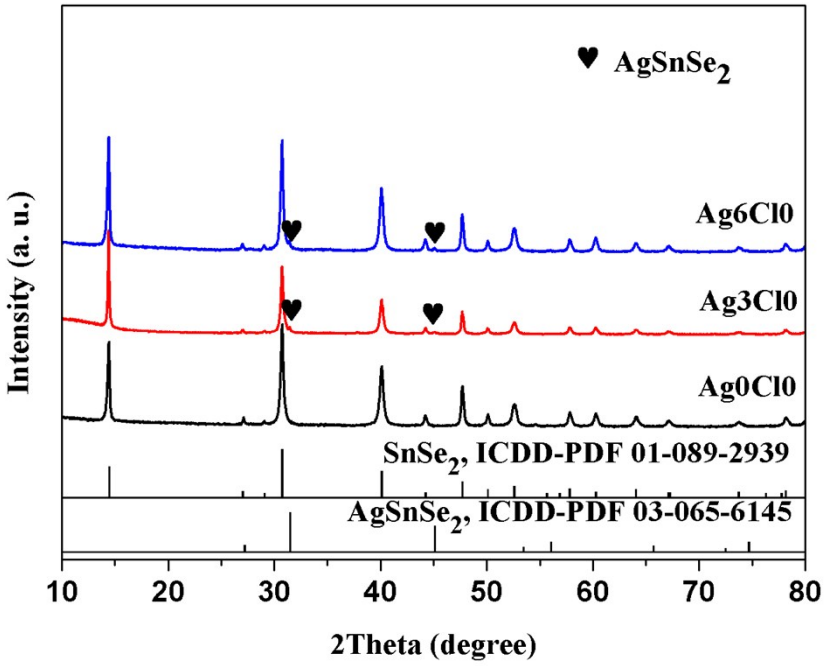


Fig. S9 XRD patterns of the sample Ag0Cl0, Ag3Cl0 and Ag6Cl0 (grinded powders)

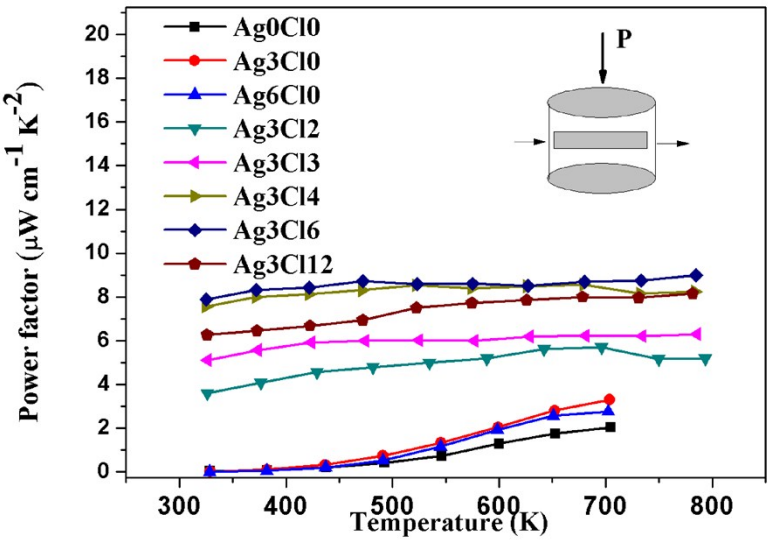


Fig. S10 Power factor of the hot-pressed samples perpendicular to the pressing direction.

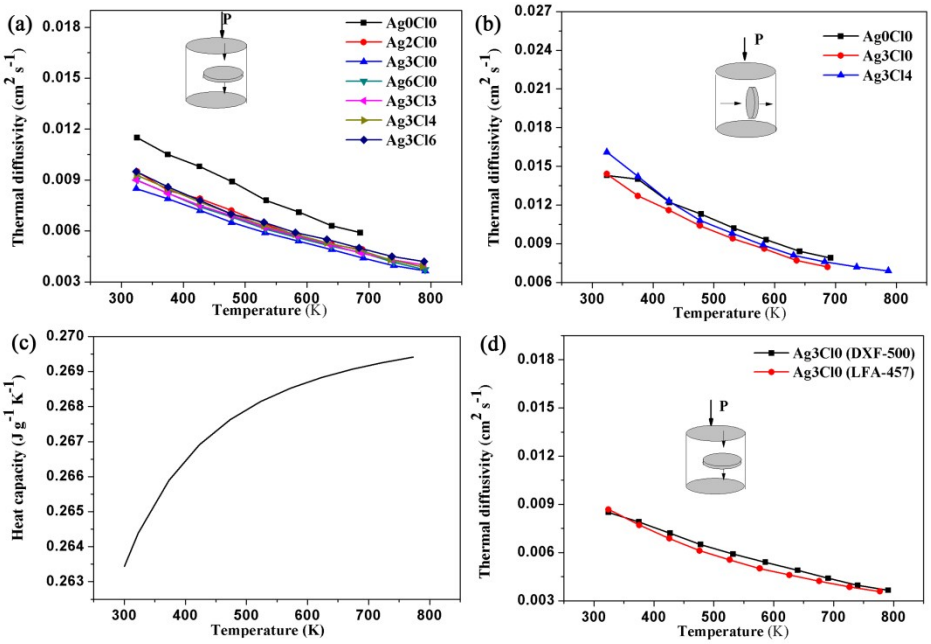


Fig. S11 Temperature-dependent thermal diffusivity (a) along the pressing direction, (b) perpendicular to the pressing direction and (c) heat capacity (Ag3Cl4). (d) The comparison of thermal diffusivity (Ag3Cl0) measured by the instrument DXF-500 and LFA-457.

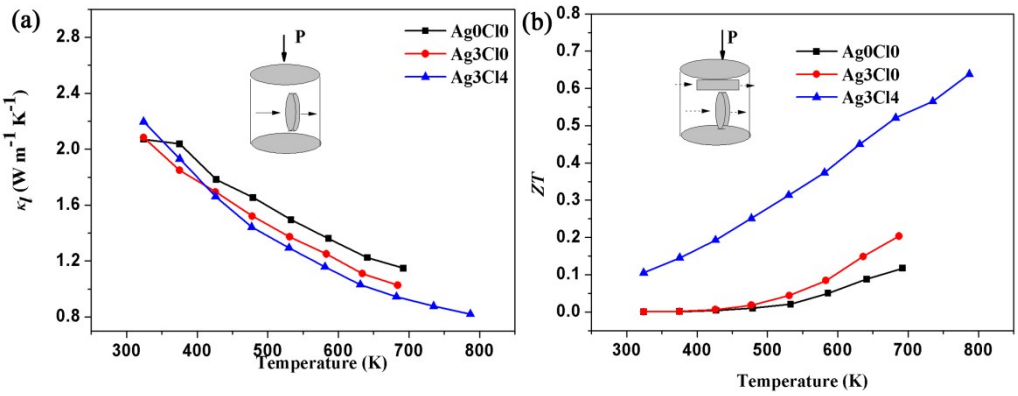


Fig. S12 (a) Lattice thermal conductivity and (b) *ZT* of the hot-pressed samples perpendicular to the pressing direction.

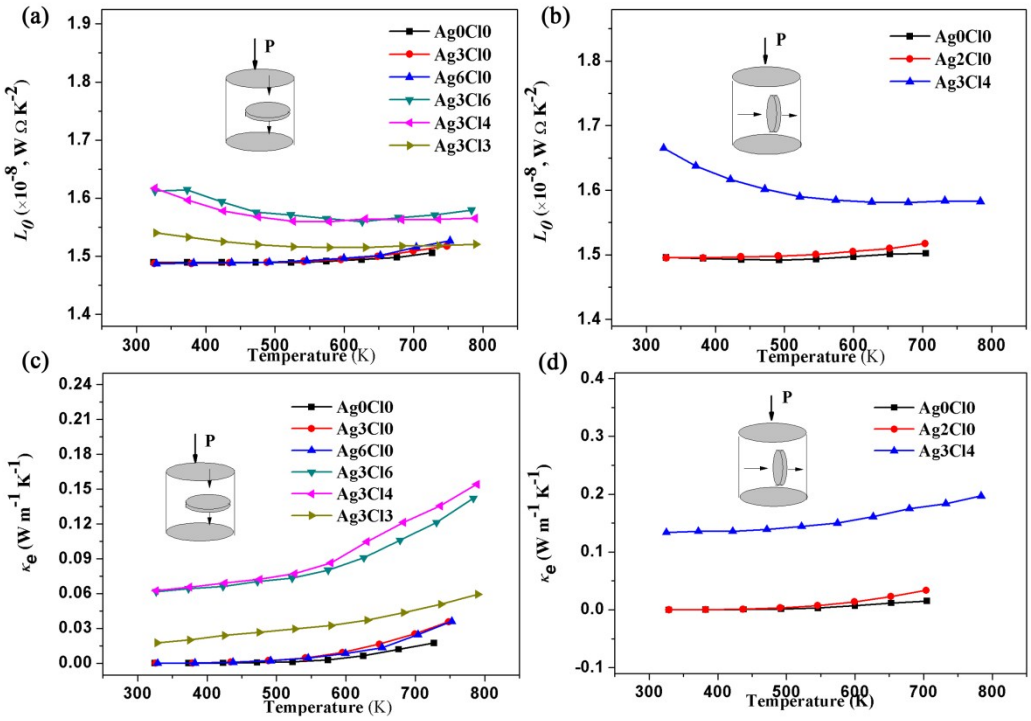


Fig. S13 Temperature-dependent Lorenz number ($L_0$) and electronic thermal conductivity ($\kappa_e$) of the hot-pressed samples (a, c) along and (b, d) perpendicular to the pressing direction.

**The calculation of $L_0$**

Assuming the acoustic phonon scattering dominates the carrier scattering mechanism, which indicates $r$ = -1/2, the Lorenz number ($L_0$) can be estimated by the following equations

$$L_0 = \left(\frac{k_B}{e}\right)^2 \frac{3F_0(\eta)F_2(\eta) - 4F_1(\eta)^2}{F_0(\eta)^2} \quad (1)$$

$$S = \frac{k_B}{e}\left[\frac{2F_1(\eta)}{F_0(\eta)} - \eta\right] \quad (2)$$

$$F_n(\eta) = \int_0^{+\infty} x^n (e^{x-\eta} + 1)^{-1} dx \quad (3)$$

where $k_B$ is the Boltzman constant, $e$ is the electron charge, $\eta$ is reduced Fermi energy $\eta = E_F/k_BT$, $F_n(\eta)$ is the Fermi integration, which can be derived from the measured $S$ on the basis of single band approximation.

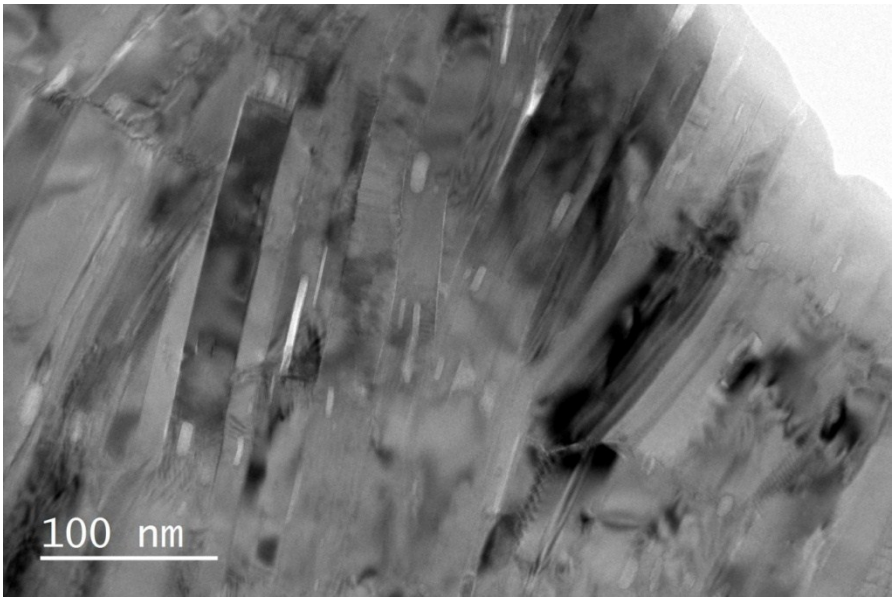


Fig. S14 A typical low-magnified TEM image of the sample Ag3Cl0.

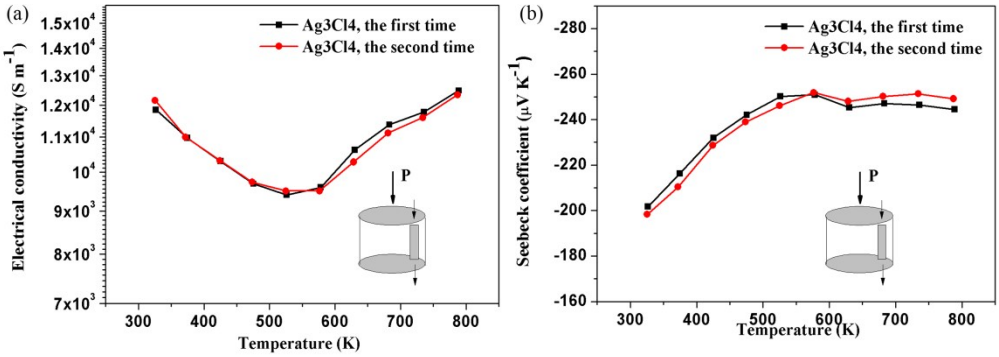


Fig. S15 (a) Electrical conductivity and (b) Seebeck coefficient of the sample Ag3Cl4 along the pressing direction collected by repeated heating measurement.

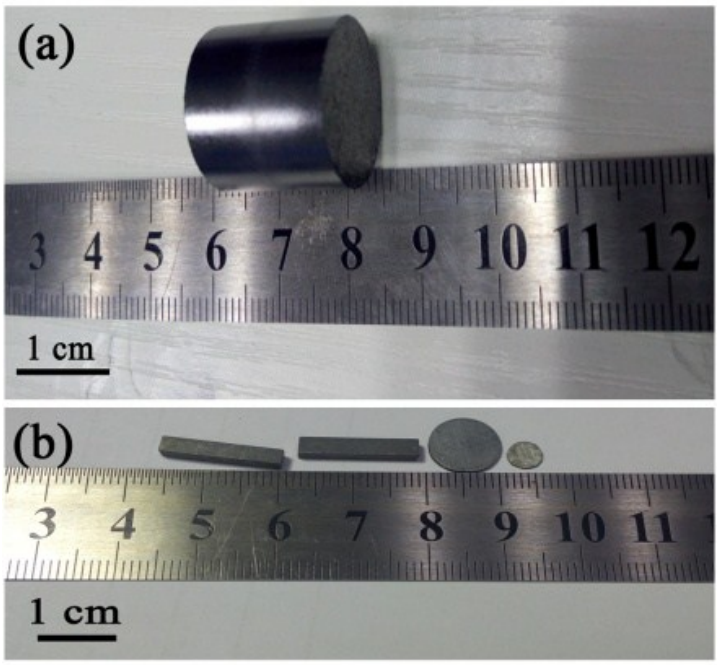


Fig. S16 Photographs of (a) a hot-pressed cylinder and (b) the corresponding cut and polished square bar and disks for the measurement of electrical and thermal transport, respectively.

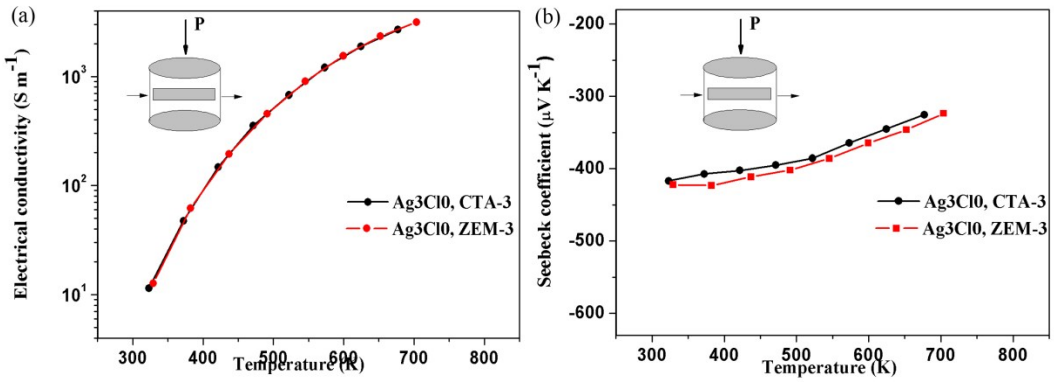


Fig. S17 Experimental data comparison of (a) electrical conductivity and (b) Seebeck coefficient between the instrument ZEM-3 and CTA-3 for the sample Ag3Cl0.

**The Lotgering method**

The orientation degree of the hot-pressed cylinders is calculated by the Lotgering method performed on the (00*l*) crystal planes, which is termed as $F_{(00l)}$ and estimated by the following equations

$$F = \frac{P - P_0}{1 - P_0} \qquad (4)$$

$$P_0 = \frac{I_0(00l)}{\sum I_0(hkl)} \quad (5)$$

$$P = \frac{I(00l)}{\sum I(\mathrm{h}kl)} \quad (6)$$

where $P_0$ and $P$ present the ratios of the integrated intensity of all (00$l$) crystal planes to those of all the ($hkl$) crystal planes. In the present work, the $P_0$ and P are calculated by using the stardard PDF card (JCPDS no. 01-89-2939) and the XRD data shown in Figure 2a, respectively. The results are given in Table SI.

Table S1. The orientation degree of the hot-pressed samples.

| Samples | $P_{(00l)}$ | $F_{(00l)}$ |
|---|---|---|
| Ag0Cl0 | 0.37 | 0.21 |
| Ag3Cl0 | 0.44 | 0.29 |
| Ag3Cl2 | 0.40 | 0.24 |
| Ag3Cl3 | 0.44 | 0.29 |
| Ag3Cl4 | 0.42 | 0.27 |
| Ag3Cl6 | 0.55 | 0.43 |

1 S. Saha, A. Banik, K. Biswas, *Chem. Eur. J.* 2016, **22**, 15634.

2 C. H. de Groot, C. Gurnani, A. L. Hector, R. M. Huang, M. Jura, W. Levason, G. Reid, *Chem. Mater.* 2012, **24**, 4442.

3 A. J. Smith, P. E. Meek, W. Y. Liang, *J. Phys. C: Solid State Phys.* 1977, **10**, 1321.